



HAL
open science

Stress-assisted versus strain-induced martensites formed by cryogenic ultrasonic shot peening in austenitic stainless steels

Marc Novelli, Pierre Maurel, Laurent Weiss, Thierry Grosdidier, Philippe Bocher

► To cite this version:

Marc Novelli, Pierre Maurel, Laurent Weiss, Thierry Grosdidier, Philippe Bocher. Stress-assisted versus strain-induced martensites formed by cryogenic ultrasonic shot peening in austenitic stainless steels. International Conference of Shot Peening ICSP-13, 2017, Montréal, Canada. hal-02455075

HAL Id: hal-02455075

<https://hal.science/hal-02455075>

Submitted on 28 Jan 2020

HAL is a multi-disciplinary open access archive for the deposit and dissemination of scientific research documents, whether they are published or not. The documents may come from teaching and research institutions in France or abroad, or from public or private research centers.

L'archive ouverte pluridisciplinaire **HAL**, est destinée au dépôt et à la diffusion de documents scientifiques de niveau recherche, publiés ou non, émanant des établissements d'enseignement et de recherche français ou étrangers, des laboratoires publics ou privés.

Stress-assisted versus strain-induced martensites formed by cryogenic ultrasonic shot peening in austenitic stainless steels

M. Novelli ^{a,b,c}, P. Maurel ^{a,b,c}, L. Weiss ^a, T. Grosdidier ^{a,b}, P. Bocher ^c

^aLaboratoire d'Etude des Microstructures et de Mécanique des Matériaux, marc.novelli@univ-lorraine.fr, pierre.maurel@univ-lorraine.fr, laurent.weiss@univ-lorraine.fr, thierry.grosdidier@univ-lorraine.fr, France;

^bLABoratoire d'EXcellence Design des Alliages Métalliques pour Allègement de Structures, France ;

^cEcole de Technologie Supérieure de Montréal, Canada, philippe.bocher@etsmtl.ca

Keywords: surface modification, cryogenic shot peening, martensite, severe plastic deformation

Introduction

Severe plastic deformation (SPD) is used to create nanocrystalline metallic materials resulting in high strength but associated, generally and unfortunately, with a reduced ductility [1]. On one side, the cryogenic temperature that improves the grain refinement by preventing dynamic recrystallization or self-annealing, has been used during SPD processes such as equal channel angular extrusion (ECAE) or high pressure torsion (HPT), effectively producing significant extra grain refinement down to the nanometer scale [2–4]. On the other side, numerous research works have been done to improve the low ductility by creating multi-length scale structures [5] or grain size gradients [6]. In steels, other mechanisms can be active and lead to a significant improvement of the strength/ductility balance such as TRIP (Transformation Induce Plasticity) [7] or the TWIP (TWinning Induced Plasticity) [8] effects.

In the case of the metastable austenitic stainless steel, the TRIP effect is produced through the martensitic phase transformation. The martensitic transformation requires an activation energy to be triggered which can be produced either thermally or by a mechanical loading. Two temperatures, the M_s and M_{d30} , are used to evaluate the occurrence of the martensitic transformation. The M_s temperature represents the temperature at which the martensitic phase transformation can be triggered spontaneously without an external loading. By applying a loading, the transformation can take place at higher temperatures than M_s and the stress or strain required to activate the process will vary with the temperature [9]. The M_{d30} temperature, higher than the M_s , reflects the temperature at which a martensitic fraction of 50% can be formed under a true strain of 30 %. When the martensitic phase transformation is triggered slightly higher than the material M_s temperature, elastic stresses in the microstructure are enough to activate the transformation and the elastic energy induced in the material is enough to compensate the missing chemical driving force at this temperature [11]. On the other hand, when the deformation is applied close to the material M_{d30} temperature, the transformation will be mainly controlled by plastic deformation and the role of deformation defects will control the transformation process [10]. The so-formed martensites can then be considered as different and called Stress-Assisted Martensite (SAM) and Strain-Induced Martensite (SIM), respectively.

On the other hand, TWIP can happen when Stacking Fault Energies (SFE) is in the range 18-45 mJm⁻² for austenitic structures. Deformation twinning is especially promoted by high strain rate. The α' martensite can be produced at the intersection of mechanical twins as this volume is double-sheared, resulting in the nucleation of the phase: $\gamma \rightarrow \gamma$ (twins) $\rightarrow \alpha'$. In the case of lower SFE (<18 mJm⁻²), martensitic transformation can involve the formation of a transient phase named ε -martensite. The formation of the ε -martensite is driven by the insertion of Shockley partial dislocations in every two successive $\{111\}_\gamma$ plans [13]. The face-centered cubic austenite is consequently transformed in the hexagonal close-packed ε -martensite as they share their same atomic packing factor. Thus, under increasing loading, the ε -martensite will act as a transient phase to produce the more stable α' martensite as follows: $\gamma \rightarrow \varepsilon \rightarrow \alpha'$.

As the SFE is also reduced when the temperature switch from a value close to M_{d30} to one close to M_s temperatures, the martensitic transformation that followed a strain-induced transformation sequence $\gamma \rightarrow \gamma$ (twins) $\rightarrow \alpha'$ can then follow a stress-assisted transformation sequence $\gamma \rightarrow \varepsilon \rightarrow \alpha'$. As the Fe-Cr-Ni austenitic stainless steels studied in this contribution are characterized by low M_s temperatures and low Stacking Fault Energies (SFE) [12] it is expected that some modification of the transformation mechanisms and sequence may happen depending on the deformation temperature.

On a practical point of view and as failure is often initiated from the surface, different SPD techniques have been developed to superficially deformed the mechanical components and consequently enhance the surface properties of materials. Among the techniques, the one derived from the conventional pre-strain shot peening has been used with much longer treatment durations. This technique is called by different names, the most commons being Surface Mechanical Attrition Treatment (SMAT) or Ultrasonic Shot Peening (USP) [14,15]. The major difference between the USP and the conventional shot peening lies in the fact that, instead of projecting the treatment media in a uniaxiale direction, the shots are here set in motion within a confined chamber and have a wide variety of incidence angles when colliding onto the surface. Thus, after a sufficiently large number of impacts, many different slip systems are activated, leading ultimately to a significant grain size refinement - down to the sub-micrometer range - and a substantial hardening of the surface and subsurface. Cryogenic temperature (CryoT) was also used with this method to improve the refinement of the top surface layer [16] or modify the in-depth (sub-surface) hardening behavior [17].

Objectives

The aim of the present manuscript is to determine the effect of the SFE of different austenite matrix under SMAT. To this end, two types of austenitic stainless steels with different SFE values were deformed at two different temperatures. The first alloy is the highly stable 310S stainless steel which, because it should remain austenitic under loading, was used as a reference. The second one is the metastable 304L stainless steel which is expected to undergo the martensitic transformation under loading. It was found that by applying the SMAT deformation at different temperatures, Room Temperature (RT) or Cryogenic Temperature (CryoT), the degree of metastability was changed and induced different deformation mechanisms.

Methodology

Cylindrical samples, 30 mm in diameter and 10 mm in thickness, were polished down to a mirror like finish to prevent any surface martensitic transformation from grinding prior to shot peening, especially for the 304L stainless steel. The SMAT experiments were conducted during 20 min with a sonotrode vibrating amplitude of 60 μm and a frequency of 20 kHz using an equipment developed by the SONATS company [18]. To conduct the cryogenic temperature experiments, a sample holder was equipped with a liquid nitrogen cooler allowing the sample to be kept at a stable temperature of -130°C during the shot peening treatment procedure.

The initial 310S and 304L steels, having an austenitic grain size of 80 μm and 30 μm , are characterized by a hardness of 170 HV and 210 HV, respectively. The alloy chemical compositions are presented in Table 1. The differences in austenitic thermal stability and their ability to transform in martensite are materialized in Table 1 through their M_s and M_{d30} temperatures calculated with the formulas given by Angel [19] and Pickering [20]. For the 310S alloy, the $M_{d30} = -169^\circ\text{C}$ is extremely low and reflects the stability of this alloy. Comparatively, the low stability of the 304L is reflected by the $M_{d30} = 21^\circ\text{C}$ and $M_s = -130^\circ\text{C}$ values. In this alloy, the martensitic transformation is expected to take place at room temperature or with relatively low level of strain under cryogenic condition.

Vickers microhardness measurements were made with traditional filiations on the cross section (50 gr with 50 μm step size). X-Ray Diffraction (XRD) analyses were run to identify the phase transformations as a function of the depth from the peened surface using a Cobalt K_{α} source. Microstructure analysis was conducted using Scanning Electron Microscopy (SEM) and Electron BackScatter Diffraction (EBSD), the EBSD maps presented here were made at a magnification of x1000 with a 0.1 μm step size.

Table 1: Compositions of the 310S and 304L steels and associated M_{d30} [19] and M_s [20] values

	C [wt.%]	Cr	Ni	Mn	Mo	N	P	Si	S	M_s	M_{d30}
310S	0.046	24.59	19.20	1.50	0.25	0.024	0.027	0.44	0.002	X	-169°C
304L	0.025	18.11	8.01	1.54	-	0.68	0.034	0.45	0.002	-130°C	21°C

Results and discussion

The microhardness measurement results are summarized in Figure 1 as a function of the depth from the surface and for both alloys. The continuous lines display the results after a peening treatment carried out at RT whereas the dash lines are for the CryoT peening. The two horizontal dotted lines represent the hardnesses of the as-received materials. The arrows are used to indicate the depths at which the XRD analyses (Figure 2) were carried out in the 304L, the solid ones for the RT treatment and the open ones for the cryogenic conditions.

For both temperatures, the 310S displays very similar hardness profiles. The only slight difference being that from a depth of 200 μm , the hardness for the CryoT treated sample is lower than the RT deformed sample. Thus there is no benefit for the stable 310S to be treated at CryoT.

For the 304L steel, the hardness values at the surface are similar for the two temperatures, but below 50 μm , the subsurface behavior differs between 100 μm and 400 μm . Indeed, the subsurface hardness resulting from the CryoT peening treatment is substantially enhanced compared to the one obtained at RT. An increase of about 100 HV is even obtained between 200 and 250 μm . Eventually, at a depth of 400 μm , the hardness of the CryoT treated sample falls slightly earlier toward the as-received value.

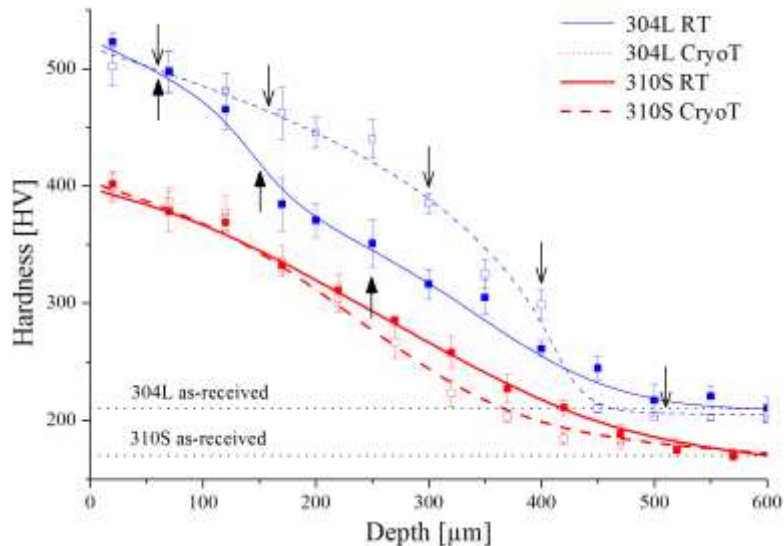


Figure 1 : Microhardness as a function of the depth on 310S and 304L at Room Temperature (RT) and Cyogenic Temperature (CryoT). The arrows are used to indicate the depths at which the XRD analyses (Figure 2) were carried out.

Figure 2 compares the XRD diffractograms obtained at different depths on the 304L samples treated both at RT (Figure 2a) and CryoT (Figure 2b). The depths at which the XRD analysis were carried out are written along the XRD traces in Figure 2 and highlighted by arrows in Figure 1. At RT, the

surface layer and sublayers contained a martensitic phase which was only of the α' -type. Below 100 μm , the volume fraction of α' -martensite reduces, as the distance from the treated surface increases, to the favor of the γ -austenite phase. No α' -martensite was observed below 250 μm and the hardness increase is only due to dislocation density. Comparatively, at CryoT 32% of α' -martensite is still present 400 μm below the surface. At this depth, the XRD diffractograms also reveal the presence of slight amounts of another type of martensite: the ε -martensite.

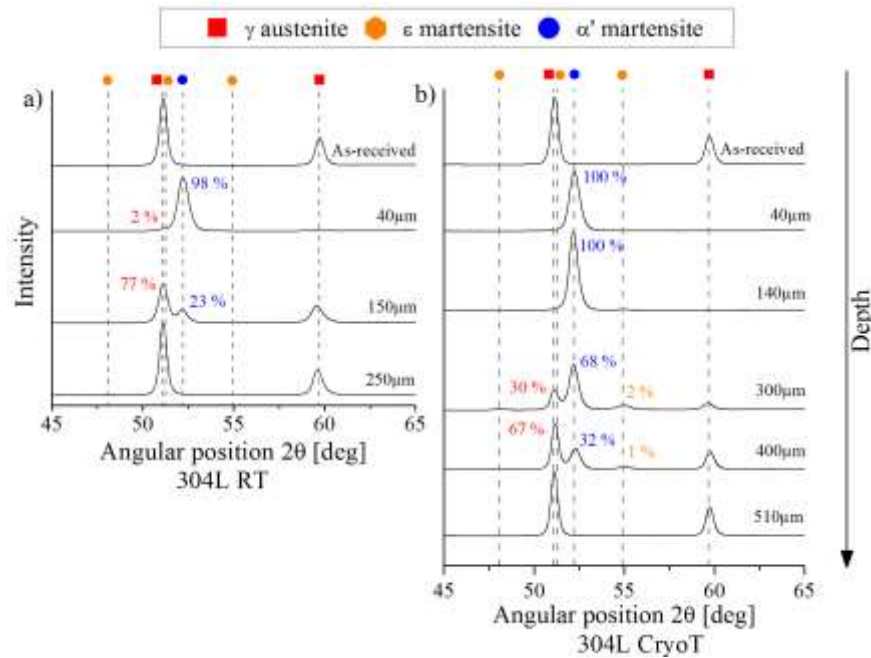


Figure 2 : X-Ray Diffraction spectrograms of 304L at a) RT and b) CryoT showing the amount of phase detected at different depths below the surface.

In order to have a better understanding of the differences in terms of phase transformation behavior, EBSD imaging was conducted in the 304L at depths for which both, γ -austenite and α' -martensite are present, facilitating the observations of the transformation behaviors between the two treatment temperatures. The EBSD acquisitions are shown in Figure 3 where the austenite is represented in band contrast, the $\{111\}_{\gamma}$ 60° twin relation in red, the α' -martensites in blue and the ε -martensite in orange. The grain boundaries lower than 10° are plotted in white principally to make the α' -martensite variants visible. The opened triangles in the close-view are here to help the readers locating the ε -martensite.

The image of the RT sample (Figure 3a) shows parallel elongated α' -laths crossing the grains from one side to the other. In addition, the red lines drawn in the figure materialize the presence of $\{111\}$ mechanical twins. The presence of these two features indicates that SIM martensitic transformation: $\gamma \rightarrow \gamma$ (twin) $\rightarrow \alpha'$ has taken place. Similar observations were done by Chen et al. [21] at a depth of 100 μm in their analysis of the 304L steel SMATed under high energy condition. Comparatively, in the CryoT sample acquisition (Figure 3b), twin relationships are rarely found and ε -martensite was detected in small quantities at the vicinity of the α' -martensite, confirming the XRD results. The ε -martensite is always located near the α' -martensite phase as alternate layers (see close-view in Figure 3b). This is a typical aspect of the SAM $\gamma \rightarrow \varepsilon \rightarrow \alpha'$ transformation.

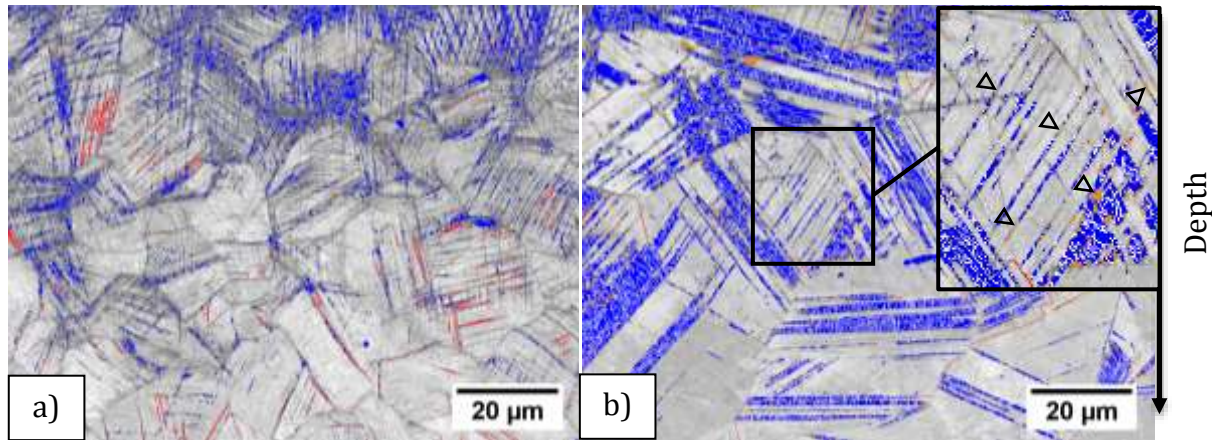


Figure 3 : EBSD images of the 304L transition layers after a) a RT and b) a CryoT treatment. The austenite is represent in band contrast, the $\{111\}_\gamma$ 60° twin relationships in red, the α' -martensite in blue and the ϵ -martensite in orange. The opened triangles in the close-view are here to help the readers locating the ϵ -martensite.

As it has been shown by Horiuchi et al. [22], austenitic stainless steels are subjected to an increase of the yield strength when cooled down to cryogenic temperatures. Concerning the 310S and the 304L, the study has revealed that their yield strengths increase from 380 MPa to 700MPa for the 310S alloy and from 220 MPa to 380 MPa for the 304L when the temperature is reduced from RT to CryoT, leading to increases of 184% and 173%, respectively. On one hand, if the martensitic phase transformation cannot be triggered (like the 310S) the increase in yield limit under cryogenic temperature will prevent the plastic deformation to take place; thus reducing the effect of the shots on the subsurface region of the part being treated (in other words, reducing the hardness). On the other hand, the ability of the austenite to undergo the martensitic transformation in the 304L is enhanced, not only by reducing the amount of plastic deformation required for the transformation due to the lower temperature, but also due to the change in the deformation mechanism related to the lowering of the material SFE. Thus, at CryoT, the higher metastability of the austenite (as it can be activated through the stress-assisted transformation) results in a significantly higher amount of martensite in the subsurface region, which in turn enhances the subsurface hardening of the 304L alloy. At depth where the stress produced by the shots is too low to trigger the stress-assisted transformation, the hardness drops rapidly to the level of the initial material, and a reduction of the affected layer thickness is observed compared to RT.

From the XRD analysis and EBSD acquisitions, the existence of differences between the RT and CryoT treatments for the 304L was confirmed in terms of deformation mechanisms. At RT, the strain resulting from the SMAT treatment will deform they-austenite by activating dislocations and twins (as in 310S), and afterward transform into α' -martensite. A typical strain-induced transformation sequence will take place for intermediate SFE whereas in lower SFE processing condition the martensitic transformation will include ϵ -martensite in a stress-assisted manner and subsequently transform into α' -martensite under an increasing stress levels or strain amount.

Conclusions

In this work, two different austenitic steels were studied after RT and cryogenic SMAT to characterize the effect of the austenite metastability on the produced deformed microstructure. For the highly stable 310S steel processed under cryogenic condition, the subsurface hardness was decreased compared to the RT treatment, revealing the absence of interest on cryogenically deformed this type of alloy by SMAT. Comparatively, a substantial increase in the metastable 304L subsurface hardness was produced by the decrease in treatment temperature. These opposite behaviors between the two alloys was attributed to the easier formation of martensite in the 304L steel subsurface due to the lower stacking fault energy of the alloy.

Furthermore, while the stress-assisted martensitic transformation was observed at CryoT (following the $\gamma \rightarrow \varepsilon \rightarrow \alpha'$ transformation sequence), only a strain-induced transformation was produced in the 304L alloy treated at RT.

Acknowledgements

This work was partly supported by the French State through the program "Investment in the future" operated by the National Research Agency (ANR) and referenced by ANR-11-LABX-0008-01 (Labex DAMAS). The authors are also thankful to the Frontenac scholarship program for supporting the author (MN) thesis.

References

- [1] R.Z. Valiev, Y. Estrin, Z. Horita, T.G. Langdon, M.J. Zehetbauer, Y.T. Zhu, *Fundamentals of Superior Properties in Bulk NanoSPD Materials*, *Mater. Res. Lett.* 3831 (2015) 1–21.
- [2] K. Edalati, J.M. Cubero-Sesin, A. Alhamidi, I.F. Mohamed, Z. Horita, Influence of severe plastic deformation at cryogenic temperature on grain refinement and softening of pure metals: Investigation using high-pressure torsion, *Mater. Sci. Eng. A.* 613 (2014) 103–110.
- [3] K. Edalati, T. Daio, M. Arita, S. Lee, Z. Horita, A. Togo, I. Tanaka, High-pressure torsion of titanium at cryogenic and room temperatures: Grain size effect on allotropic phase transformations, *Acta Mater.* 68 (2014) 207–213.
- [4] V. V. Popov, E.N. Popova, A. V. Stolbovskiy, V.P. Pilyugin, Thermal stability of nanocrystalline structure in niobium processed by high pressure torsion at cryogenic temperatures, *Mater. Sci. Eng. A.* 528 (2011) 1491–1496.
- [5] Y.M. Wang, E. Ma, Three strategies to achieve uniform tensile deformation in a nanostructured metal, *Acta Mater.* 52 (2004) 1699–1709.
- [6] T.H. Fang, W.L. Li, N.R. Tao, K. Lu, Revealing extraordinary intrinsic tensile plasticity in gradient nano-grained copper., *Science.* 331 (2011) 1587–90.
- [7] O. Grässel, L. Krüger, G. Frommeyer, L.W. Meyer, High strength Fe-Mn-(Al, Si) TRIP/TWIP steels development - properties - application, *Int. J. Plast.* 16 (2000) 1391–1409.
- [8] O. Bouaziz, S. Allain, C. Scott, Effect of grain and twin boundaries on the hardening mechanisms of twinning-induced plasticity steels, *Scr. Mater.* 58 (2008) 484–487.
- [9] G.B. Olson, M. Cohen, Kinetics of strain induced martensitic nucleation, *Met.* 6 A (1975) 791–795.
- [10] F. Lacroix, A. Pineau, Martensitic Transformations Induced By Plastic-Deformation in Fe-Ni-Cr-C System, *Metall. Trans.* 3 (1972) 387–396.
- [11] G.B. Olson, M. Cohen, A mechanism for the strain-induced martensitic transformations nucleation of, *Met.* 28 (1972) 107–118.
- [12] R.E. Schramm, R.P. Reed, Stacking fault energies of seven commercial austenitic stainless steels, *Metall. Trans. A.* 6 (1975) 1345–1351.
- [13] P.M. Kelly, The martensite transformation in steels with low stacking fault energy, *Acta Metall.* 13 (1965) 635–646.
- [14] K. Lu, J. Lu, Nanostructured surface layer on metallic materials induced by surface mechanical attrition treatment, *Mater. Sci. Eng. A.* 375–377 (2004) 38–45.
- [15] J. Azadmanjiri, C.C. Berndt, A. Kapoor, C. Wen, Development of Surface Nano-Crystallization in Alloys by Surface Mechanical Attrition Treatment (SMAT), *Crit. Rev. Solid State Mater. Sci.* 40 (2015) 164–181.
- [16] K.A. Darling, M.A. Tschopp, A.J. Roberts, J.P. Ligda, L.J. Kecskes, Enhancing grain refinement in polycrystalline materials using surface mechanical attrition treatment at cryogenic temperatures, *Scr. Mater.* 69 (2013) 461–464.
- [17] M. Novelli, J.-J. Fundenberger, P. Bocher, T. Grosdidier, On the effectiveness of surface severe plastic deformation by shot peening at cryogenic temperature, *Appl. Surf. Sci.* 389 (2016) 1169–1174.
- [18] <http://www.sonats-et.fr>
- [19] T. Angel, Formation of martensite in austenitic stainless steels, effects of deformation, temperature and composition., *J. Iron Steel Inst.* (1954) 165–175.
- [20] F.P. Pickering, Physical metallurgy and the design of steels, *Appl. Sci. Publ.* (1978).
- [21] A.Y. Chen, H.H. Ruan, J. Wang, H.L. Chan, Q. Wang, Q. Li, J. Lu, The influence of strain rate on the microstructure transition of 304 stainless steel, *Acta Mater.* 59 (2011) 3697–3709.

- [22] T. Horiuchi, R. Ogawa, M. Shimada, S. Tone, M. Yamaga, Y. Kasamatsu, Mechanical properties of high manganese steels at cryogenic temperatures, *Adv. Cryog. Eng. Mater.* (1982) 93–103.